

3D outcrop geologic modeling applied to test the role of brittle structures on permoporosity of poorly lithified reservoirs

Camila Faria de Albuquerque^{1,2*} , Aline Theophilo Silva² , Mathieu Moriss³ , Claudio Limeira Mello¹ 

Abstract

Poorly lithified siliciclastic rocks correspond to important post-salt reservoirs in the Southeastern Brazilian Margin offshore basins. These reservoirs present challenges regarding the prediction of the hydraulic behavior of faults due to low cohesion leading to diffuse brittle deformation. To improve the understanding of the deformation influence on the reservoir quality of these rocks, this paper presents a 3D modeling method based on an outcrop analog composed of Paleogene poorly lithified fluvial siliciclastic deposits in the Volta Redonda Basin (Continental Rift of Southeastern Brazil). A database was collected containing a 3D digital terrain model of the outcrop, a 1:50-scale geological section, permeability and porosity measurements, and lithological and sonic log from a well drilled upon the outcrop to the basement. Two models were built: one using traditional methods for industry where properties were uniformly distributed throughout the grid and a second model where sectors were delimited and populated with data from deformed rocks, highlighting the impact of tectonic structures (faults and deformation bands) on fluid flow, reducing the permeability by one order of magnitude, and increasing the flow time between wells by more than 10%. This study contributes to improving reservoir modeling accuracy, enhancing the understanding of fluid flow behavior in complex, deformed, poorly lithified rocks.

KEYWORDS: poorly lithified sandstone; analog reservoir modeling; digital outcrop; fractured reservoir.

1 INTRODUCTION

Predicting reservoir fluid behavior during production is one of the most important challenges in the oil industry. As hydrocarbon reservoirs rarely outcrop, integrated analyses combining indirect data (e.g., well logs, seismic data) and direct data (e.g., whole cores, core plug samples, sidewall core samples) are required to support several reservoir development operations. All these data are incomplete since acquisition is not done systematically because the wells are drilled in the most productive reservoir areas, and not all possible data are collected from every well. Also, direct data acquisition is particularly expensive and time-consuming. Ultimately, the database necessary to reach a good comprehension of the reservoir fluid behavior is not always available.

The use of outcrops as analogs to hydrocarbon reservoirs has proven to be a powerful tool for improving subsurface reservoir models, as it provides information on a sub-seismic scale that allows qualitative and quantitative assessment of

dimensions and geometries of sedimentary units, facies distributions, tectonic structures, and lateral and vertical discontinuities (Howell et al., 2014).

When focusing on brittle deformed, poorly lithified sandstones (high porosity and low cohesion sandstones), the scenario is even more complex due to the scattered nature diffuse character of the deformation in this type of rock. As faults can behave as conduits, barriers, or combined barrier-conduit structures for hydrocarbon migration, their presence increases the risks for hydrocarbon drilling, exploration, and development (Pei et al., 2015). However, faults in poorly lithified sandstones frequently present little displacement, and their damage zone thicknesses are variable, making them unidentifiable on seismic (resolution of 15-20 m). Deformation band zones are also a common tectonic feature in poorly lithified sandstones (Fossen et al., 2007), and they occur dispersed throughout the sandy layers, making it impossible to identify them when using seismic data. Despite the difficulty in detecting deformation features in poorly lithified sandstones, their presence has a significant impact on the reservoir's permoporous properties, and the diffuse character of the deformation represents a specific challenge for fluid flow prediction.

Poorly lithified sandstone reservoirs are very important targets for the post-salt Brazilian hydrocarbon plays (Fetter et al., 2009), representing a significant contribution to Brazil oil reserves. For example, the most important poorly lithified sandstone reservoir in the Campos Basin has already produced 1.4 billion barrels and represents the third-largest field in total accumulated oil production (ANP, 2021). Despite this, few studies have focused on deformation in outcrop analogs to these

¹Universidade Federal do Rio de Janeiro – Rio de Janeiro (RJ), Brazil. E-mails: albuquerquecf@yahoo.com.br, limeira@geologia.ufrj.br

²Petrobras – Rio de Janeiro (RJ), Brazil. E-mails: camilafaria@petrobras.com.br, alinet@petrobras.com.br

³Aspentech – Rio de Janeiro (RJ), Brazil. E-mail: mathieu.moriss@aspentech.com

*Corresponding author.

This document has an erratum: <https://doi.org/10.1590/2317-488920240029ERRATUM>



rocks, and outcrop studies have not been integrated with real reservoirs (Araujo et al., 2018; Balsamo et al., 2010; Bezerra et al., 2017; Pontes et al., 2019; Vogel et al., 2019). The few examples where this integration has been done focus on consolidated rocks and their permoporous characterization, thus ignoring fault behavior (Bongiolo & Scherer, 2010; Rodrigues, 2018; Rodrigues & Silva, 2018; Soweck, 2013).

The present study aims to build a 3D geologic grid that integrates the stratigraphical and structural frameworks and lithologic and petrophysical data from an outcrop of faulted poorly lithified rocks. These deposits are considered geomechanically analog to some low-cohesion post-salt sandstone reservoirs in the Campos Basin, which frequently present deformation bands and subseismic faults. This work is intended to highlight the effect of the tectonic structures on the fluid flow dynamics within this kind of reservoir.

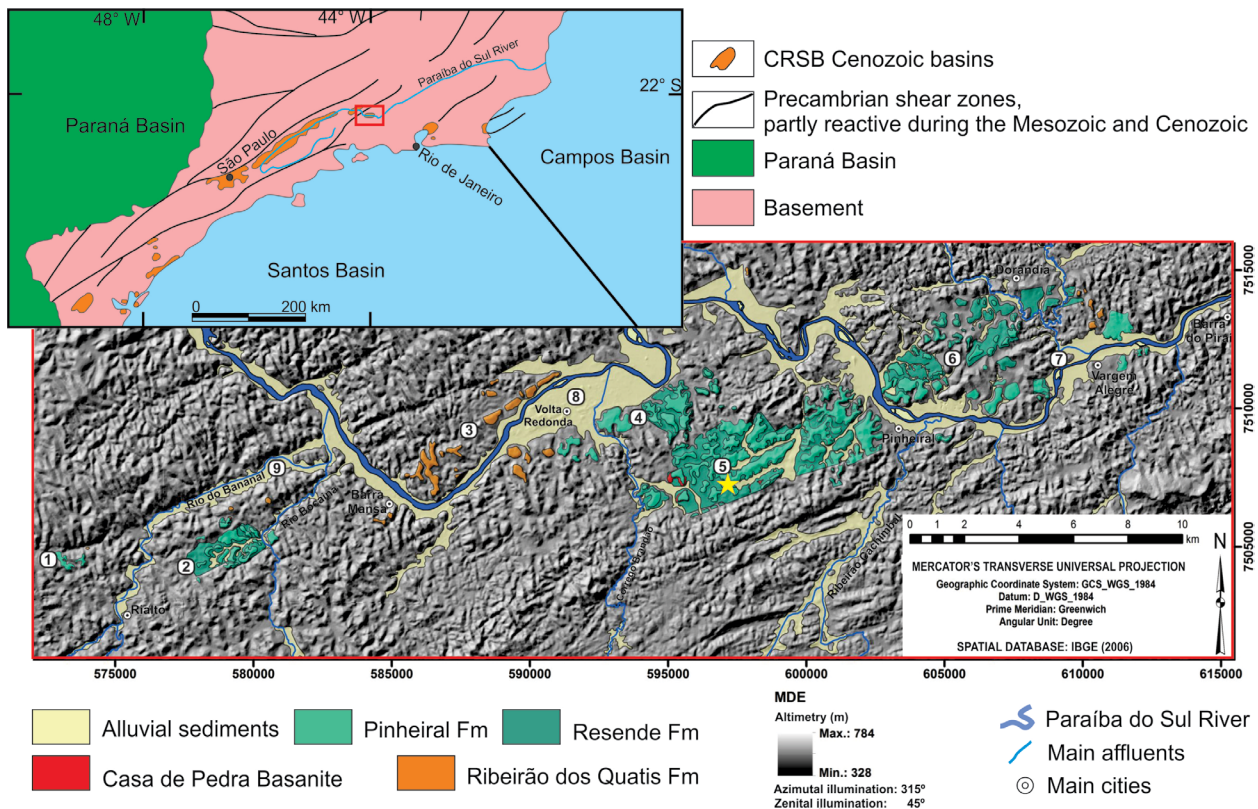
2 GEOLOGICAL SETTING

The studied outcrop is located in the Volta Redonda Basin (Fig. 1), which is part of the central segment of the Continental Rift of Southeastern Brazil (CRSB) that corresponds to an ENE-WSW Paleogene tectonic feature developed along the Southeastern Brazilian margin for nearly 900 km (Riccomini, 1989; Riccomini et al., 2004). According to these authors, the tectonosedimentary evolution of the CRSB central segment started with the formation of a continuous hemigraben as the result of an Eocene NNW-SSE distensive stress field (E1 event) that caused the reactivation as a normal fault

of NE-SW to ENE-WSW Neoproterozoic basement shear zones. As described by several authors (Negrão et al., 2020; Riccomini, 1989; Riccomini et al., 2004; Sanson, 2006), the stratigraphical record in the Volta Redonda Basin that is associated with this tectonic event is composed of alluvial fan and braided river deposits (Resende Formation) and also includes alkaline ultramafic volcanic rocks (Casa de Pedra Basanite). The Paleogene stratigraphical record also includes braided fluvial deposits of the Ribeirão dos Quatis Formation (Pre-Rift) and of the Pinheiral Formation, which was deposited in a disconformity over the Resende Formation and Casa de Pedra Basanite (Negrão et al., 2020). Above the Paleogene units, there are Quaternary colluvial and alluvial deposits.

Four deformational tectonic events are recognized throughout the CRSB central segment and involve reactivations along preexisting faults and the generation of new structures (Riccomini et al., 2004). These events correspond to (1) Miocene E-W sinistral strike-slip tectonics (TS), with NW-SE extension and NE-SW compression; (2) Pleistocene to Holocene E-W dextral strike-slip tectonics (TD), with NW-SE compression and NE-SW extension; (3) Holocene WNW-ESE extension; and, finally, (4) modern E-W compression.

Compared to the other basins of the CRSB central segment, the Volta Redonda Basin is the smallest of them, both in area and thickness, and the most deformed. According to Negrão et al. (2015), there are three main Paleogene depocenters in this basin: Colônia Santo Antônio, Dorândia, and Casa de Pedra grabens. The latter is the most important depocenter due to its sedimentary and volcanic record.



Source: Modified from Negrão et al. (2015).

Figure 1. Map of the Cenozoic sedimentary units of the Volta Redonda Basin over the relief shading model, emphasizing the strong control of the distribution of Paleogene deposits by NE-SW structures and, subordinately, NW-SE structures. The yellow star indicates the location of the studied outcrop.

The outcrop here studied is located very close to the southern border of the Casa de Pedra Graben (Fig. 2) and is composed of extensive lenticular to tabular feldspathic sandstones interbedded with conglomerates and mudstones, corresponding to deposits of the Resende Formation (Eocene). The outcrop is divided into two slopes (upper and lower), and there are two major ENE-WSW-trending normal faults (F1 and F2) with opposite dips and throws around 5 m and 8 m, respectively (Fig. 2). These faults are related to the E2 event, and they are associated with the reactivation of previous strike-slip faults generated in TS and/or TD events (Maciel et al., 2017). They split the outcrop into three compartments: southern, central, and northern sectors. Sandstones and conglomerates are the predominant lithologies in the southern sector, and most of the deformation band zones are identified in this sector. The central sector represents a graben, with sandstones and greenish mudstones, and minor faults. The northern sector is characterized by conglomerates, sandstones, and a few mudstone layers. On the top of the outcrop, there are conglomerates and sandstones of the Pinheiral Formation.

3 MATERIALS AND METHODS

The dataset used in this study comprises a digital terrain model (DTM) produced from remotely piloted aircraft system's high-quality orthophotographs, a 1:50-scale geological section, in-situ permeability measurements, porosity

and permeability measurements obtained in the laboratory, and the lithological profile and the acoustic log from the well 2-VR-0001-RJ drilled from the top of the outcrop to the basement. From this dataset, it was possible to build a 3D geologic model and property models (lithology, porosity, and permeability).

The DTM was produced by Lima (2017) and has 5 cm precision in a 100 m high flight. The 1:50-scale geologic section of the outcrop (Fig. 3) was produced by Mello et al. (2021) and records seven main lithologies (claystone, siltstone, muddy sandstone, fine sandstone, medium to coarse sandstone, conglomerate, and intraformational breccia), faults, and deformation bands zones.

The in-situ permeability data comprises more than 5,000 measurements collected by Andrade (2020) and Galvão (2018) on the outcrop using a TinyPerm3 mini-permeameter with no confining pressure conditions. Data acquisition was guided by a regular 2×2 m grid along the geologic section (Fig. 3), and the measurements were done in three orthogonal directions (two horizontal and one vertical). The horizontal readings were obtained parallel and perpendicular to the main faults (F1 and F2). The authors collected more than ten permeability readings in each orthogonal direction by each cell grid to guarantee the best accuracy of the median value calculated for each direction.

The porosity and permeability data obtained in the laboratory correspond to petrophysical measurements performed

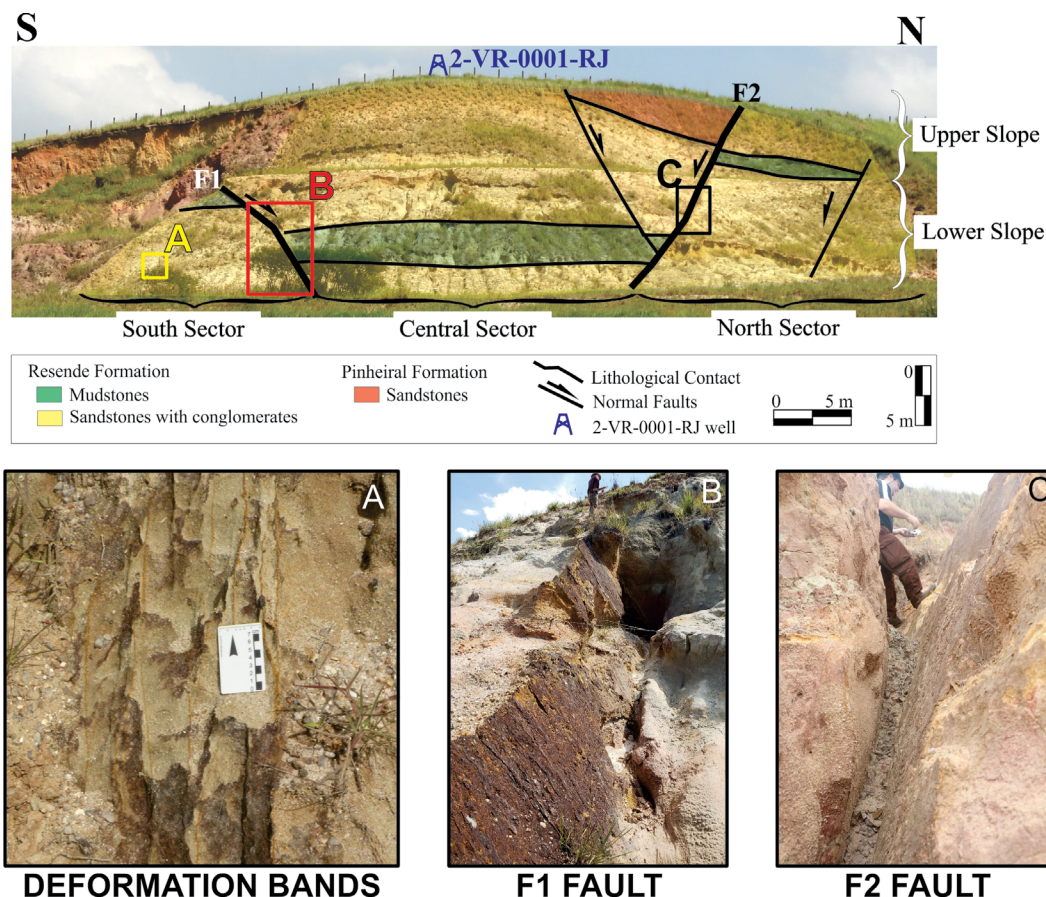


Figure 2. General aspects of the studied outcrop, showing the main lithologic contacts and the most tectonic structures. The photographs highlight the location of the main tectonic structures present in the outcrop: (A) the deformation bands in the southern sector, (B) the ferruginized plane of Fault F1, and (C) the presence of clay smear on Fault F2.

by Galvão (2018), Mello et al. (2021) and Vogel (2018) from plugs extracted at the lower slope of the outcrop. These plugs were analyzed at confining pressure conditions of 2,000 psi.

The well 2-VR-0001-RJ was drilled at the top of the outcrop, and it reached the basement at 65 m depth. An acoustic log was run into this well, in addition to other logs (caliper, spontaneous potential, resistivity, and natural gamma ray), and a whole core was made. From this whole core, Mello et al. (2021) did a 1:20-scale lithological description that is used in the present study.

The workflow followed to build the 3D geologic model (Fig. 4) comprehends two major steps: (1) build the outcrop virtual model (OVM) using the point cloud and the orthophotographs generated by Lima (2017), and (2) build the geologic model using the OVM to extrapolate the surfaces to construct the structural and stratigraphical frameworks. A 3D triangulated surface was produced using the point cloud and the orthophotographs were draped onto this surface to generate the OVM. These steps were done using Aspentech SKUA-GOCAD, version 2020.

The orthophotographs were analyzed in Adobe Photoshop and SKUA-GOCAD, using the “tiff” and “geotiff” formats, to avoid loss of resolution as it can occur in other formats. Photoshop displays better resolution and color definition, but it is only possible to observe the orthophotograph in two dimensions. On the other hand, SKUA-GOCAD allows manipulating the image in a three-dimensional environment; however, it degrades the resolution. Both software were used to compare color definitions, texture, and stratigraphic surfaces on the orthophotographs to identify stratigraphical horizons and tectonic structures to produce the interpreted OVM. This interpreted OVM was validated in the outcrop where the dip and azimuth directions of the surfaces were measured to support the three-dimensional modeling.

After interpreting the stratigraphical horizons, it is important to define the stratigraphical column and understand their chronological and spatial relationships (e.g., erosive, intrusive, or conformable contacts; onlap, downlap, toplap, or truncated surfaces).

The volume of interest (VOI) defined to build the outcrop 3D geologic model involved the outcrop face, the well 2-VR-0001-RJ,

and an interval of 3 m width behind this well. In this VOI, stratigraphical horizons and tectonic structures (faults and deformation bands) interpreted in the OVM must be extrapolated until they reach the VOI borders. To extrapolate these surfaces, it is required to use the measurements collected in the outcrop (for example, strike/dip fault measurements). As this geologic grid will be used to simulate fluid flow, it is mandatory that one side of its cell be perpendicular to the observed groundwater flow in the area to simplify the application of Darcy’s Law.

To build the structural framework, it is necessary to set the relationship between the faults that will be represented in the geologic model (e.g., main faults and secondary faults, fault kinematics, and cross-cutting relationships). After that, it is time to generate the stratigraphical framework, considering the relationships between the stratigraphical horizons and the faults (e.g., throw and cross-cutting relationships).

When the structural and stratigraphical frameworks were built, it was possible to build the geologic model, setting the size of its cells and their orientation. For this study, the geologic model was built with a cell size of 50 × 50 cm in the horizontal directions (X and Y). For the vertical direction (Z), it was defined to be 10 cm for sandstone layers and 50 cm for muddy layers, and 1 m for the first layer (the basement). This difference in the vertical direction was used to represent the different sandstones observed in the outcrop and to reduce the computing time for the muddy layers as they will be set with constant properties.

The workflow used to populate the 3D geologic model with the reservoir properties to build the 3D geologic grid comprises

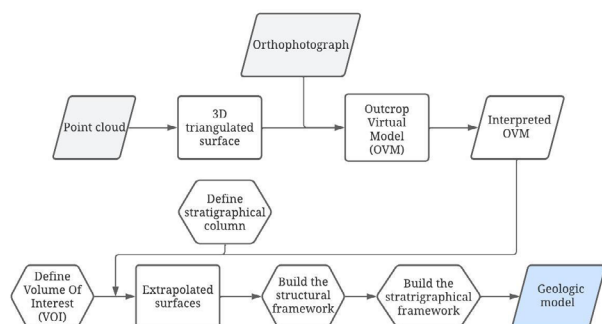
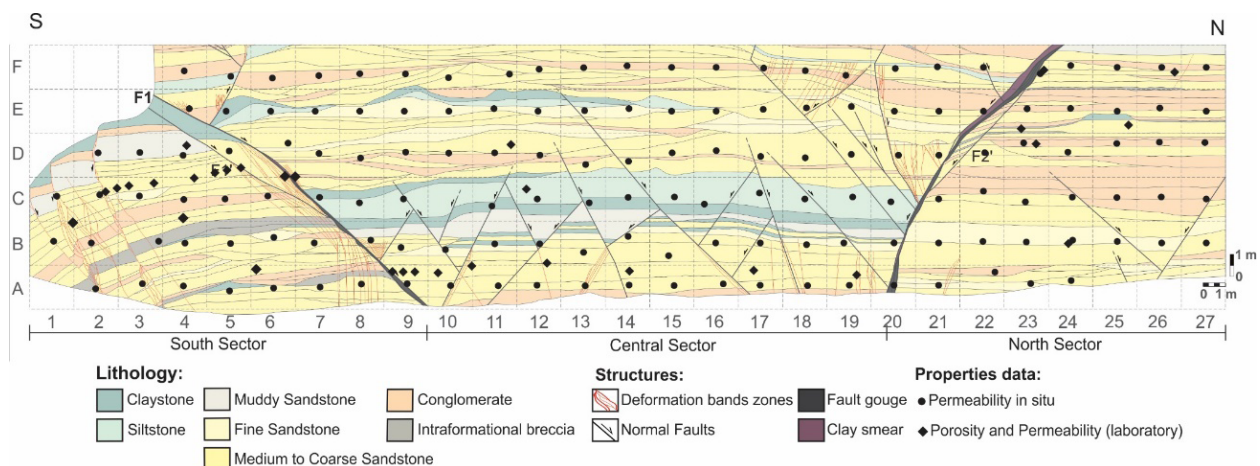


Figure 4. Workflow followed to build the geologic model.



Source: Modified from Mello et al. (2021).

Figure 3. Geologic section (original scale 1:50) of the studied outcrop lower slope with the location of porosity and permeability data.

the following major steps (Fig. 5): (1) choose the properties that will be used in the model (e.g., outcrop geologic section, well core description, permeability and porosity data, reservoir facies); (2) set the properties values on the proper position in the model; (3) define geostatistical algorithms to populate the model; (4) run calculations; (5) do quality control; and, finally, (6) the geologic grid will be ready.

The lithological dataset is composed of the outcrop geologic section and the well 2-VR-0001-RJ lithological profile. The porosity dataset is composed of the porosity measurements made in the laboratory (at 2,000 psi) and the well acoustic (porosity) log. The permeability dataset consists of the in-situ permeability data and the permeability log generated from the well porosity log. Since the in-situ permeability dataset was measured without confining pressure (0 psi), this data was treated as described in Albuquerque et al. (2024) to adapt these data to the pressure conditions (2,000 psi) usually found in post-salt reservoirs in the Campos Basin. The permeability log was generated by correlating the porosity and the permeability laboratory data, analyzing them by their reservoir facies separately (e.g., good reservoir, poor reservoir, and non-reservoir) and also with the presence of tectonic structures (e.g., non-deformed, affected by deformation bands, or by faults). The correlation equations (Fig. 6) obtained were applied to create the permeability log.

This curve was used to calculate the permeability property in the geologic grid, regardless of its direction (parallel, perpendicular, or vertical). As the intention was to have limited fluid flow through the non-reservoir facies, the permeability was set as 0.0001 mD. and a constant porosity value of 1% was used. The reservoir facies dataset was generated by combining the lithology, porosity, and permeability datasets.

It is important to set the geostatistical algorithms according to the properties that will be used, as they will directly impact the quality and the uncertainty of the geologic grid. In this study, ordinary kriging was used to build the lithological, reservoir facies, and porosity properties of the geologic grid, following the statistical procedures in the oil industry practices. As permeability has a statistical correlation to porosity, that property was applied using collocated cokriging considering porosity as the secondary data, setting the coefficient of correlation (R^2) of 0.71 for the good reservoirs, 0.36 for the poor reservoirs, 0.41 for fault regions, and 0.93 for deformation band regions, as obtained in the correlation equations (Fig. 6).

The geologic grid was built using spherical variogram models set by observations made in the outcrop. For the non-reservoir facies, the variogram was configured with $(R1) = (R2) = 100$ m to extrapolate the limits of the model while maintaining the tabularity of these layers, and $(RV) = 50$ cm. For the other

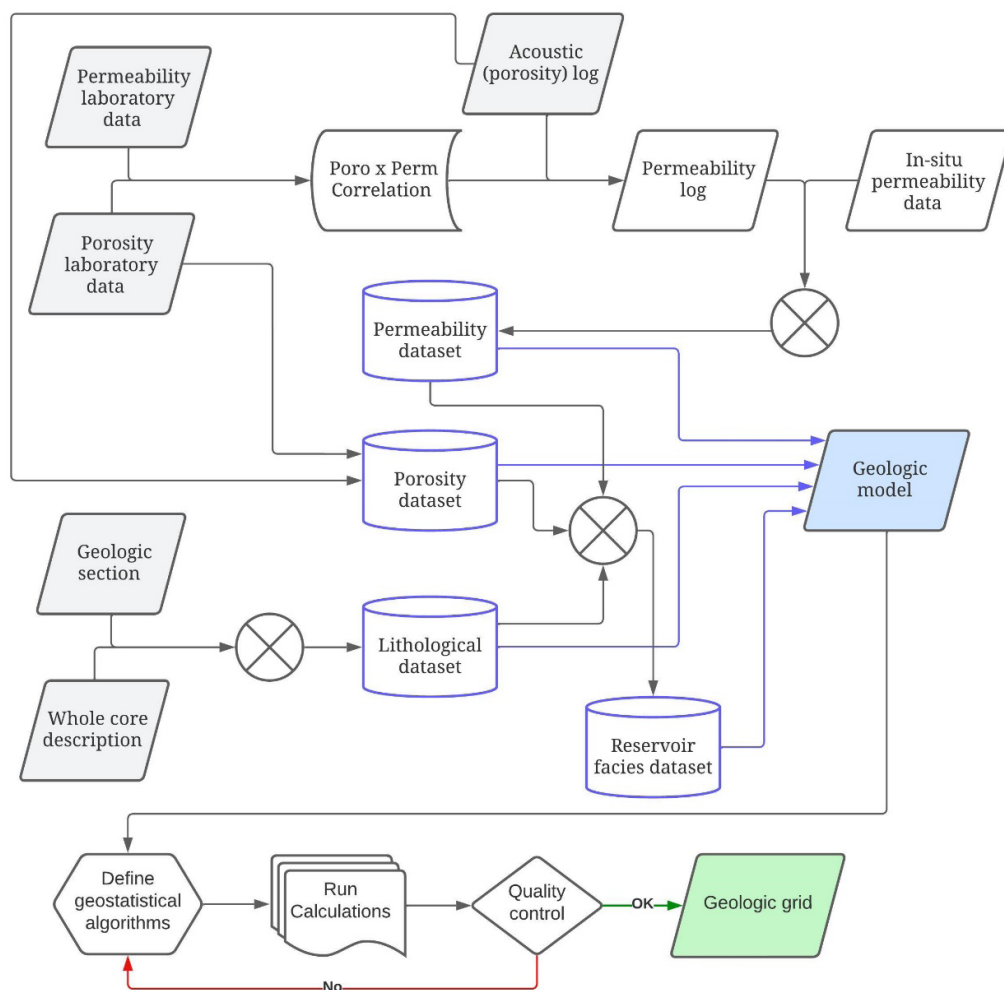


Figure 5. Workflow used to populate the geologic model with reservoir properties to build the geologic grid.

facies, the variogram model was configured with $(R1) = 25$ m, $(R2) = 100$ m, $(RV) = 50$ cm, and azimuth = 70° to reproduce the channels and paleocurrents.

To insert the lithologic property in the geologic model, the geologic section was transferred to the OVM by creating

several pseudowells (Fig. 7) and generating 1:20 lithological logs for each pseudowell. These pseudowells were replicated in the OVM surface respecting the trajectory on the outcrop topography, and the lithological log was uploaded to the software.

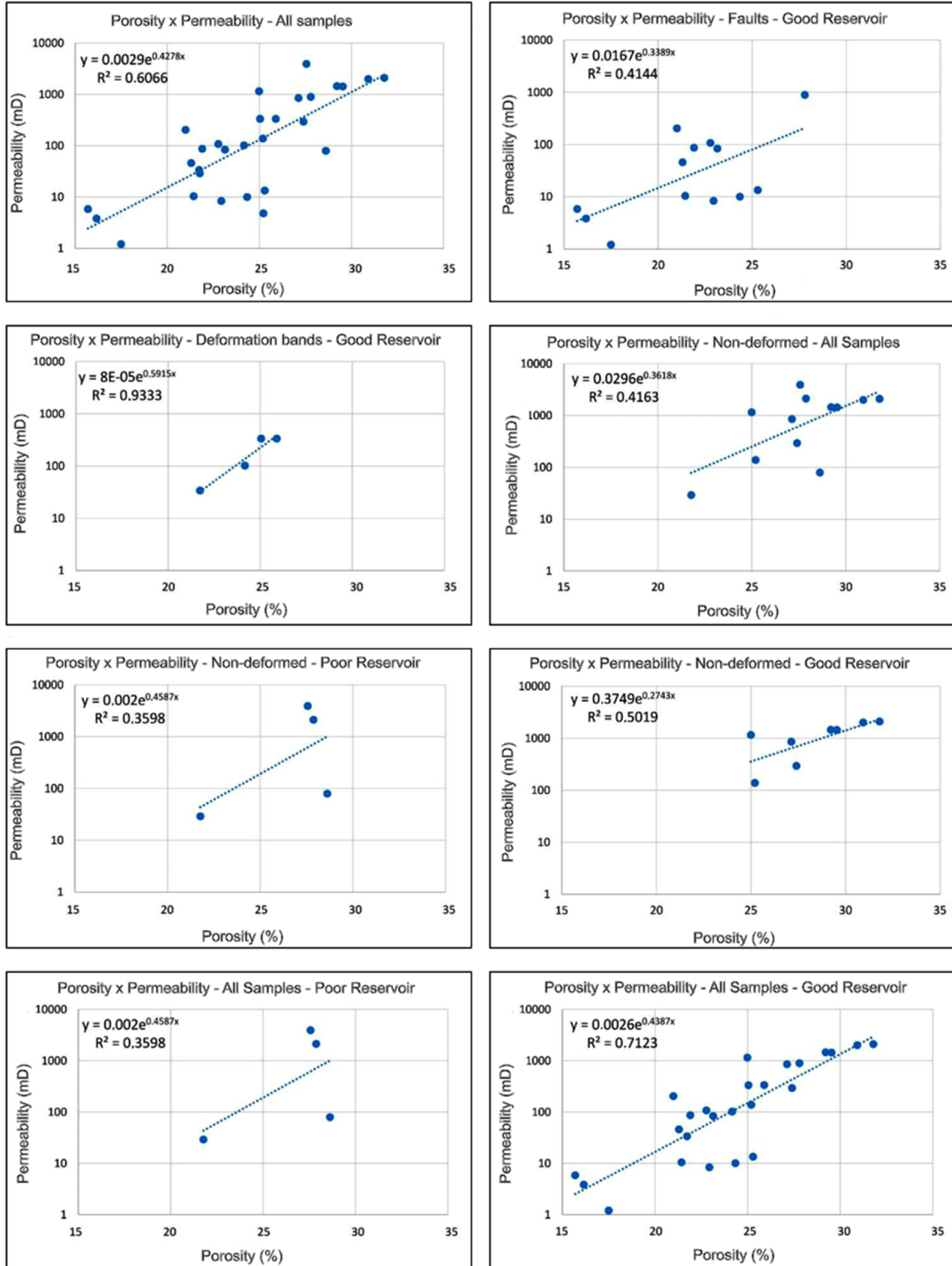


Figure 6. Correlation between porosity (%) and permeability (mD) from the samples collected in the outcrop and analyzed in the laboratory, separated by the reservoir facies and the presence of tectonic structures.

Each lithology was coded so that it could be used for modeling (e.g., claystone was marked as “1” and siltstone as “2”).

To set the lithologic property, one hundred equiprobable realizations were done, varying only the initial point in the model in that the calculation will start (seed) and keeping the other parameters (variograms and raw data). Then, it was possible to generate models of the probability of occurrence of each lithology. These models were combined and analyzed to check which lithologies were most likely to occur in each cell, resulting in the lithologic model that honors the raw data. At the end of this stage, the outcrop lithologic model is produced.

The reservoir facies property was applied using a simple script (i.e., if this... then that...) to the geologic grid with the lithologic property already set, grouping the different lithologies into classes of reservoir facies, resulting in the reservoir facies model.

To test the impact of the deformation bands and faults in the fluid flow, two models were built for each property (porosity and permeability) that impacts this flux: the first one, named here as the “standard model,” using only the data classified as non-deformed and extrapolating them into the whole model; and a second one, termed as the “sectorized model,” using the data collected in the deformed zones—corresponding to the cells located nearby the identified tectonic structures (faults or deformation bands)—then extrapolating them in the regions where these tectonic features occur.

To set the porosity property, ten different realizations were run using the same parameters, modifying only the starting seed. However, to set the permeability property and to simulate

it in the fluid flow simulation, one model was randomly chosen for each direction (perpendicular, parallel, and vertical). Different porosity and permeability truncated Gaussian distributions for each classification (facies reservoir and presence of tectonic structures) were used and applied to the respective region of the geologic grid.

After the geologic grid was finished, a fluid flow simulation was done using the Geoscreening workflow from Schlumberger Petrel 2021. The streamlined flow simulation method was used to carry out an expeditious and robust test of the fluid flow in the models to check the impact of tectonic structures on the communication time between wells inserted in the model. This method is a simplified simulation that solves the saturation equations linearly and allows a quick comparison of different scenarios (Stohler, 2021). For this study, the models had to be redesigned to a box model since the outcrop topography caused anomalies in the streamlines when the first flow simulation test was carried out. The horizons, deformation band zones, and faults were extended to the edge of the box to maintain the compartmentalization of the original model. The properties modeled in the original model were recalculated, keeping the parameters, resulting in a box model equiprobable to the original one. The streamline simulation was done for a single-phase fluid, using the default parameters of the software. The fluid considered for the simulation was oil since the purpose is to approximate the analog outcrop to reservoir conditions.

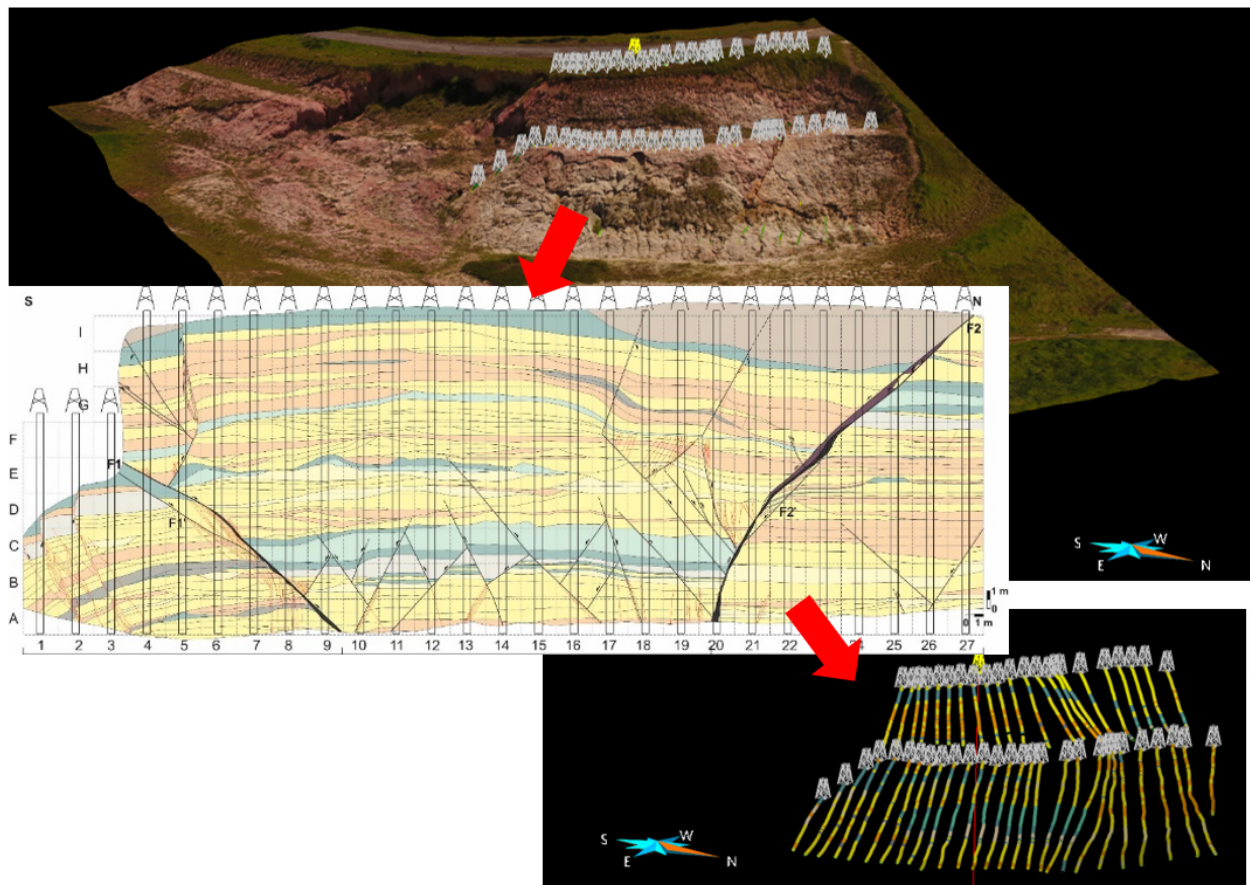


Figure 7. Pseudowells used to transport the information from the geologic section to the OVM.

4 RESULTS

4.1 Geologic model

On the orthophotographs, 15 stratigraphical horizons and 14 tectonic structures (10 faults and 4 deformation band zones) were interpreted (Fig. 8). The deformation band zones are concentrated on the southern sector of the outcrop and are rare on the other blocks. The stratigraphical horizons represent contrasts between different sedimentary intervals and do not necessarily delimit intervals of different lithologies. They are mostly horizontal and slightly irregular, which makes it possible to follow them in the three sectors. One exception is horizon 10, which truncates horizons 8 and 9 with a distinctive erosive nature. Horizons 6 and 7 represent, respectively, the bottom and the top of the main mudstone interval.

The structural and stratigraphical framework highlights the main compartments present in the outcrop. The central sector preserves the most complete stratigraphical record. The structural framework shows that faults F1 and F2 are the most important faults in the outcrop, and fault F4 is also a significant fault as it intercepts fault F1. Fault 5 was inferred when comparing the same lithological intervals in the geologic section of the outcrop and the lithological description of well 2-VR-0001-RJ.

The 3D geologic model has 112 cells in the “i” direction (horizontal direction parallel to the outcrop), 122 cells in the “j” direction (horizontal direction perpendicular to the outcrop), and 380 “cells in the “k” direction (vertical), totaling 5,192,320 cells. The 15 stratigraphical horizons delimit 16 lithological layers: layer 1 represents the base of the model, layers 2-15 represent the Resende Formation deposits, and layer 16 represents the Pinheiral Formation deposits (Fig. 9). For the Resende Formation, the colors of the model indicate the predominant lithology: the green layers are more clayish, the yellow ones are sandier, and the orange ones are more conglomeratic. Layer 16 (Pinheiral Formation) is represented in red and the model base (layer 1) in blue.

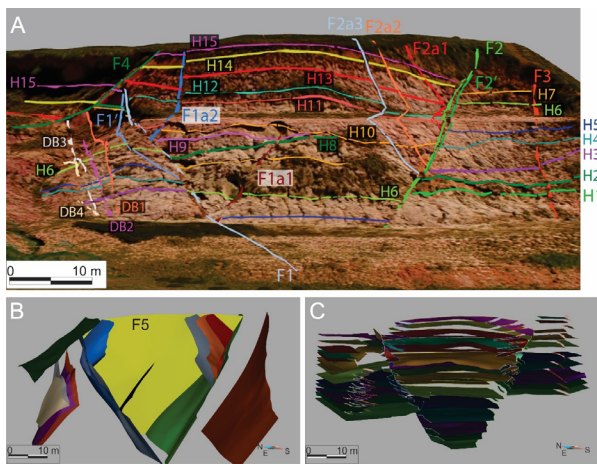


Figure 8. (A) Stratigraphical horizons (H1 to H15) and tectonic structures (deformation band zones—DB1 to DB4, and faults—F1, F1', F1a1, F2, F2', F2a1, F2a2, F2a3, F3, F4) interpreted on the OVM; (B) modeled faults and deformation bands—fault F5 was inferred by correlating the outcrop and the well; and (C) modeled horizons.



4.2 Reservoir facies

As the porosity values are very similar for the lithologies in this outcrop, this property was not determinant to classify the reservoir facies. On the other hand, the permeability values have good variability and have great consistency that allows classifying the lithology into reservoir facies. Thereby, claystone and the siltstone were grouped into non-reservoir facies; muddy sandstone and fine sandstone into poor reservoir facies; and medium to coarse sandstone, conglomerate, and intraformational breccia into good reservoir. The non-reservoir facies have an arithmetic average porosity of 27%, and an average geometric mean of the permeability of 17.3 mD; poor reservoir facies have an arithmetic average porosity of 27.2% and an average geometric mean of the permeability of 386.2 mD; and good reservoir facies have an arithmetic average porosity of 26.3% and an average geometric mean of the permeability of 4,391 mD (Table 1, Fig. 10).

When comparing the permeability values at 2,000 psi considering the location of the samples, it is possible to observe that the tectonic structures (faults and deformation band zones) reduce the permeability values by an order of magnitude (Fig. 11).

4.3 Geologic grid

The resulting lithologic model honored the geometry of the sedimentary intervals as represented in the geological section, allowing the reservoir facies model to also maintain the distribution observed for the outcrop (Figs. 12A and 12B).

Considering the porosity models (Figs. 12C and 12D), when assigning specific values for this property to the tectonic structures in the sectorized PoM2 model, it is noted that the average permeability of the model, as a whole, is reduced by

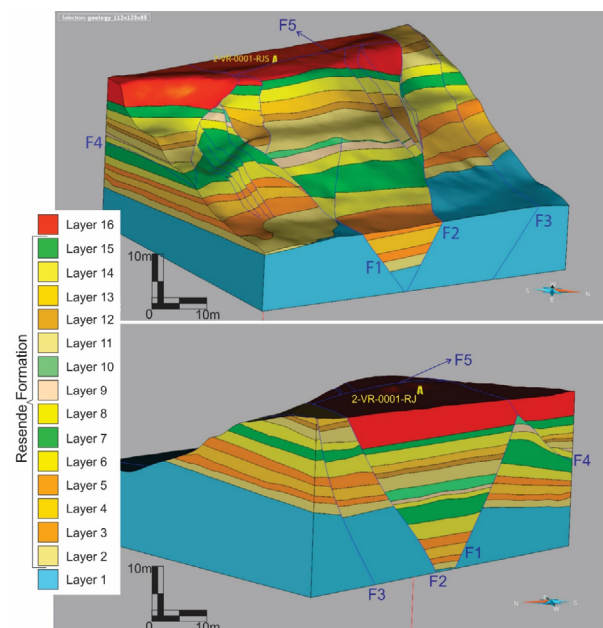


Figure 9. 3D geologic model of the investigated outcrop. (A) Front of the model. (B) Back part of the model. The Resende Formation is represented by layers 2 to 15; the green layers are more clayey, the yellow ones are sandier, and the orange ones are more conglomeratic. Layer 1 (blue) is the base of the model, and layer 16 (red) corresponds to the Pinheiral Formation. The position of well 2-VR-0001-RJ is indicated, just as the main faults (F1 to F5).

1.3% compared to the standard PoM1 model. However, when analyzing statistically the regions affected by tectonic structures, an increase of 1.1% in the porosity of the region of deformation band zones and a decrease of 13% in the porosity values in regions of faults are observed (Table 2).

For the permeability models (Figs. 12E and 12F), comparing the standard models to the sectorized models for the three directions (parallel, perpendicular, and vertical), it is observed that the tectonic structures reduce the permeability by an average of 7%. Examining the regions where these structures are, it is noted that there is a reduction of 12-30% of the permeability in the deformation band zones region and a reduction of 60-86%, in the faults region (Table 2).

4.4 Fluid flow simulation—streamlines

The fluid flow simulation was done using an injection well positioned in the south sector and a production well in the north sector, considering the viscosity for the mobilized fluid equivalent to oil. This configuration for the injector/producer pair induced the flow of fluids to pass through the F1, F1', F1a1, F1a2, F2a3, F2a2, F2a1, F2, and F2' faults and the deformation band zones, ensuring that the effect of the presence of these tectonic structures will be tested by the simulation. The fluid goes mainly through the sandy and conglomeratic layers, which can be observed due to the absence of streamlines where the main muddy layer occurs (Fig. 13). Comparing the streamlines in the standard and sectorized models, there is an increase in the tortuosity in the regions of deformation bands, zones, and faults in the sectorized model, slowing down the fluid flow by more than 13%. As a result, there is a slight increase in the washed oil production due to the turbidity time length in the reservoir cells (Table 3). In other words, with the presence of the deformation structures, the time that the injected fluid remained in each cell increased slightly, which allowed for greater remobilization of the oil contained in the reservoir towards the producing well.

5 CONCLUSION

The aim of this work was to highlight the effect of tectonic structures on fluid flow dynamics in poorly lithified sandstone reservoirs. Once the 3D outcrop models here developed were built using reliable stratigraphic and structural information and petrophysical properties of deformed and undeformed rocks,

they proved to be efficient in improving the understanding of the properties distribution and the impact of tectonic structures on this distribution.

Two types of models were built: the standard model, currently used in the oil industry, and a second one, named the sectorized model, in which the permoporosity data collected on tectonic structures were inserted into the regions where they occur. The sectorized model makes it clear that the presence of these tectonic structures has a significant impact, reducing

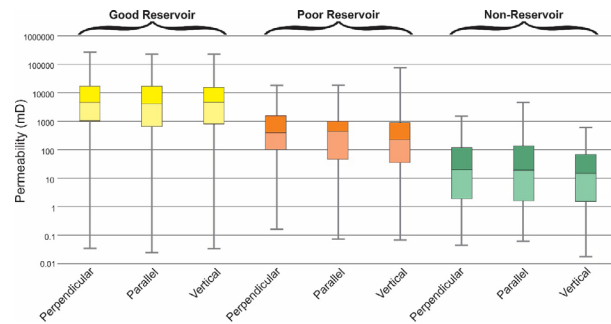
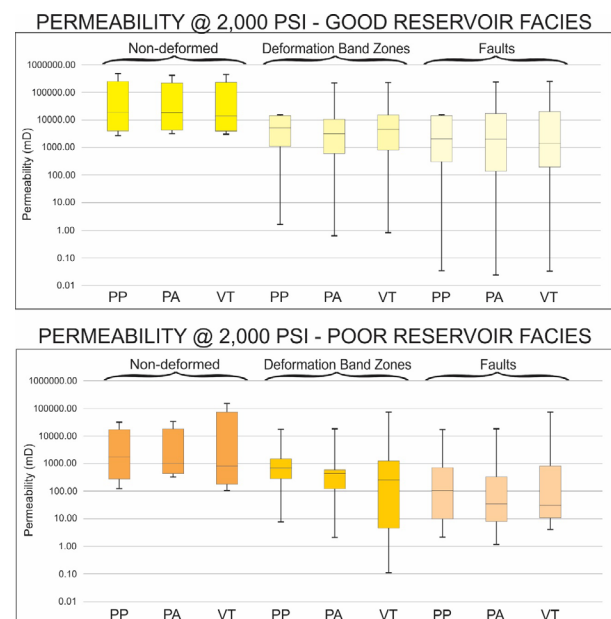


Figure 10. Box-plot graphics for the three orthogonal in-situ permeability raw data at 0 psi grouped by reservoir facies.



PP: perpendicular; PA: parallel; VT: vertical.

Figure 11. Box-plot graphics for the three orthogonal in-situ permeability @ 2,000 psi separated by their proximity to tectonic structures.

Table 1. Arithmetic mean of the porosity (%) and the geometric mean of the in-situ permeability at 0 psi separated by lithology.

Lithology	Arithmetic mean Porosity (%)	Geometric mean in-situ permeability values @ 0 psi (mD)			Reservoir facies
		Perpendicular	Parallel	Vertical	
Claystone	28.81	16	41	14	Non-reservoir
Siltstone	25.2	18	8	7	
Fine sandstone	25.78	336	183	142	Poor reservoir
Muddy sandstone	28.6	533	526	597	
Medium to coarse sandstone	26.32	2,377	1,693	1,994	Good reservoir
Conglomerate	27.11	7,842	6,928	6,378	
Intraformational breccia	25.52	8,987	2,918	399	

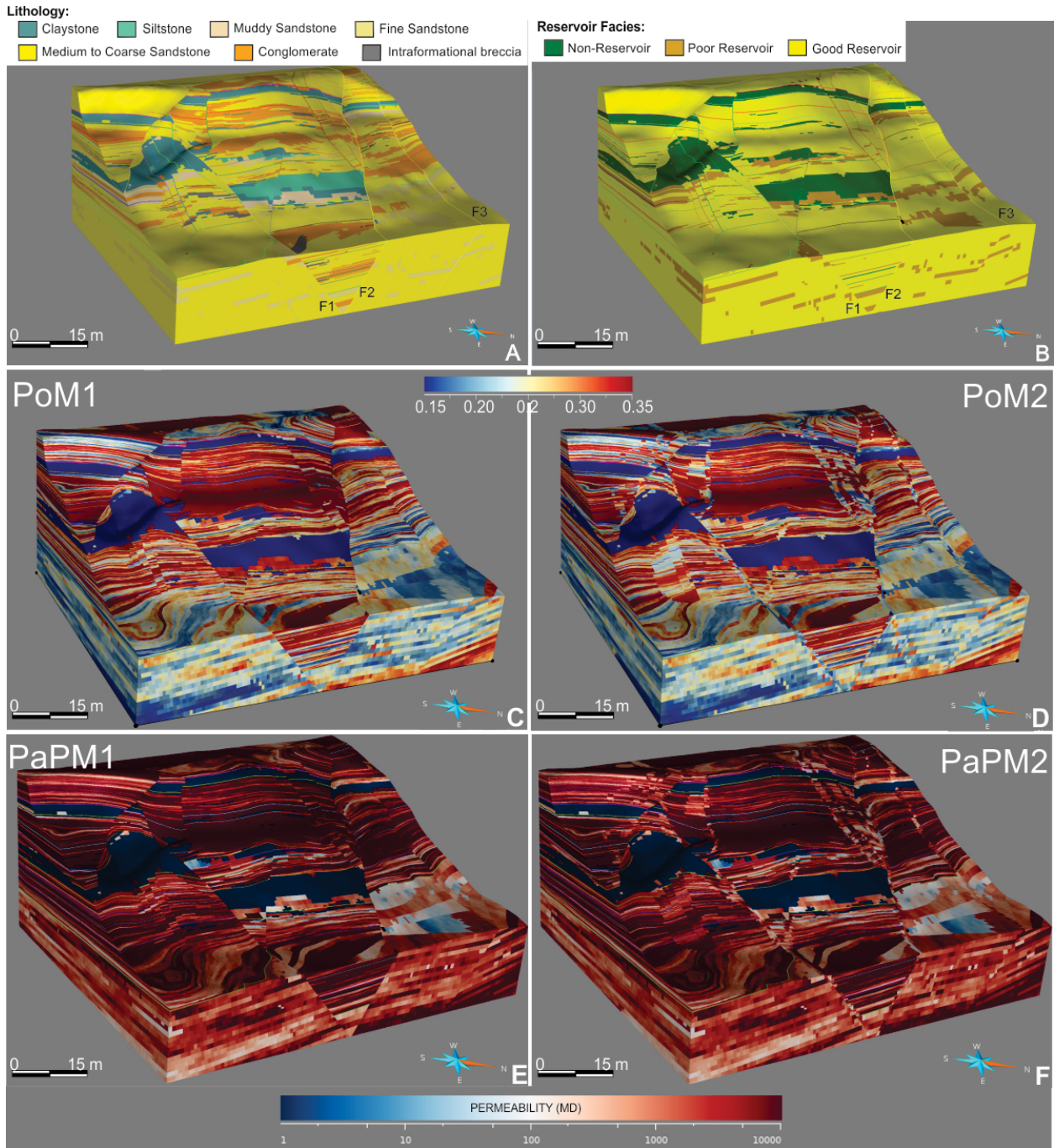


Figure 12. (A) Outcrop lithologic model and (B) reservoir facies model. (C) Standard porosity model PoM1 and (D) sectorized porosity model PoM2. (E) Standard parallel permeability model PaPM1 and (D) sectorized parallel permeability model PaPM2; the pattern is very similar in the other two directions (perpendicular and vertical) permeability models.

Table 2. Variation of the average distribution of properties (porosity and permeability) considering the sectorized model in relation to the standard model.

Property model		Porosity model (%)	Parallel permeability (mD)	Perpendicular permeability (mD)	Vertical permeability (mD)
Full model	Standard	27.77	13,780.1	15,696.9	12,229.6
	Sectorized	27.40	12,680.3	14,483.1	11,388.4
	Variation (%)	-1.32	-7.98%	-7.73%	-6.88%
Deformation band zone region	Standard	27.79	12,819.2	13,826.3	11,628.2
	Sectorized	28.09	10,218.9	9,654.02	10,192.6
	Variation (%)	+1.09	-20.28%	-30.18%	-12.35%
Fault regions	Standard	28.01	14,744.5	16,975.6	12,908.6
	Sectorized	24.40	1,992.3	2,288.9	5,066.66
	Variation (%)	-12.90	-86.49%	-86.52%	-60.75%

permeability by an order of magnitude and increasing fluid flow time between wells by more than 10%.

Although the modeled outcrop has the approximate size of only a quarter of a cell of a real reservoir model, the structural complexity found in it demonstrates the need to better understand the deformation processes effects on the poorly lithified sandstone permeability distribution. To incorporate the results here obtained on modeling routines for real reservoirs, new studies are needed to achieve

parameterizations that consider the effect of deformations on the subseismic scale.

6 ACKNOWLEDGMENTS

We would like to thank the UFRJ research team for collecting the stratigraphical, structural, and petrophysical data. We thank Petrobras for authorizing the first author's doctorate. We also thank George de Barros and Rômulo Stohler for the technical discussions.

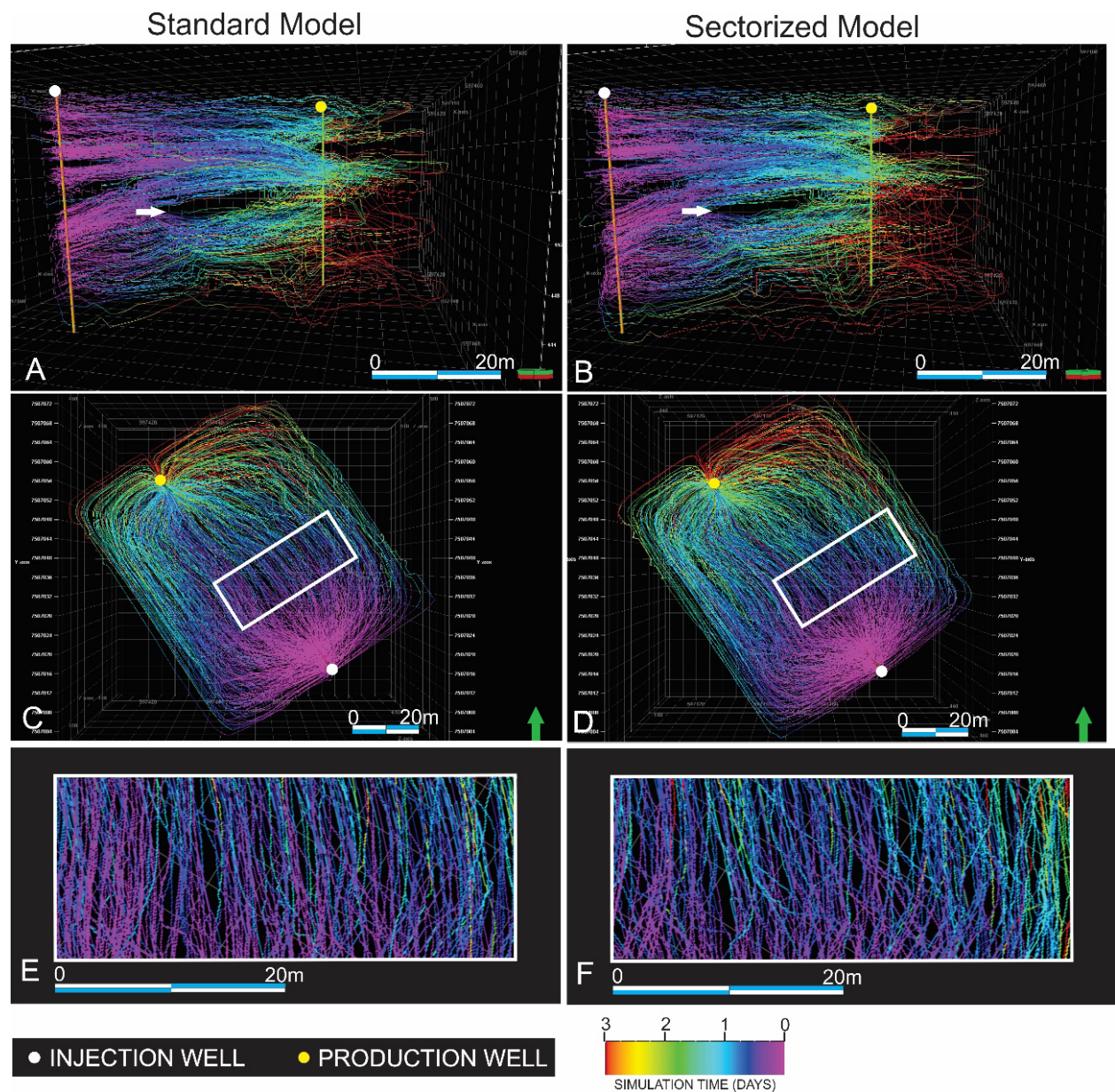


Figure 13. The streamlined simulation flow showing the “time-of-flight” using one injection well and one producing well in the standard model and in the sectorized model. (A) and (B) show that the streamlines deviate from the main muddy layer (white arrow) in both models. (C) and (D) show the map view of the time-of-flight in the two models. The white rectangles emphasize one of the regions with deformation structures (area of the F1 fault and deformation band zones), in which the flow lines are more tortuous and delayed in the sectorized model compared to the standard model. (E) and (F) show the zoom of the areas highlighted in (C) and (D), respectively.

Table 3. Variation of the “time-of-flight” (days) and oil production (m^3) considering the sectorized model in relation to the standard model.

	Standard model	Sectorized model	Variation (%)
Time-of-flight (days)	2.33	2.64	+13.30
Oil production (m^3)	18,043	18,700	+3.64

ARTICLE INFORMATION


Manuscript ID: e20240029. Received on: 18 JUNE 2024. Approved on: 24 JAN 2025. Corrected on: 19 MAY 2025.

How to cite: Albuquerque, C. F., Silva, A. T., Moriss, M. A. G., & Mello, C. L. (2025). 3D outcrop geologic modeling applied to test the role of brittle structures on permeability of poorly lithified reservoirs. *Brazilian Journal of Geology*, 55, e20240029. <https://doi.org/10.1590/2317-488920240029>

C.F.A.: Conceptualization, funding acquisition, investigation, data curation, formal analysis, methodology, investigation, project administration, supervision, validation, visualization, original draft, writing—review & editing. A.T.S.: Conceptualization, funding acquisition, data curation, formal analysis, methodology, supervision, validation, visualization, original draft, writing—review & editing. M.A.G.M.: Data curation, formal analysis, methodology, validation, visualization, writing—review & editing. C.L.M.: Conceptualization, data curation, formal analysis, methodology, supervision, validation, visualization, original draft, writing—review & editing.

Competing interests: nothing to declare.

ASSOCIATE EDITOR: Humberto Reis 

SCIENTIFIC EDITOR: Carlos Grohmann 

REFERENCES

- Albuquerque, C. F. de, Silva, A. T., & Mello, C. L. (2024). Permeability data treatment from analogous outcrop for use in three-dimensional reservoir model. *Anuário do Instituto de Geociências*, 47, 1-11. https://doi.org/10.11137/1982-3908_2024_47_59235
- Agência Nacional do Petróleo, Gás Natural e Biocombustíveis (ANP) (2021). *Boletim da Produção de Petróleo e Gás Natural*, (125). Retrieved from <https://www.gov.br/anp/pt-br/centrais-de-conteudo/publicacoes/boletins-anp/bmp/2021/2021-01-boletim.pdf>
- Andrade, T. P. (2020). *Simulação sequencial gaussiana da distribuição espacial da permeabilidade em rochas siliciclásticas pouco consolidadas e fraturadas*. Universidade Federal do Rio de Janeiro.
- Araujo, R. E. B., Bezerra, F. H. R., Nogueira, F. C. C., Balsamo, F., Carvalho, B. R. B. M., Souza, J. A. B., Sanglard, J. C. D., de Castro, D. L., & Melo, A. C. C. (2018). Basement control on fault formation and deformation band damage zone evolution in the Rio do Peixe Basin, Brazil. *Tectonophysics*, 745, 117-131. <https://doi.org/10.1016/j.tecto.2018.08.011>
- Balsamo, F., Storti, F., Silva, A. T., & Lima, C. C. (2010). Structural and petrophysical evolution of extensional fault zones in low-porosity, poorly lithified sandstones of the Barreiras Formation, NE Brazil. *Journal of Structural Geology*, 32(11), 1806-1826. <https://doi.org/10.1016/j.jsg.2009.10.010>
- Bezerra, F. H. R., Araujo, R., Maciel, I., Nogueira, F. C., Balsamo, F., Storti, F., Souza, J. A. B. de, & Carvalho, B. R. B. M. (2017). The role of major rift faults in the evolution of deformation bands in the Rio do Peixe Basin, Brazil. *19th EGU General Assembly*, p. 5438.
- Bongioiolo, D. E., & Scherer, C. M. S. (2010). Facies architecture and heterogeneity of the fluvial-aeolian reservoirs of the Sergi formation (Upper Jurassic), Recôncavo Basin, NE Brazil. *Marine and Petroleum Geology*, 27(9), 1885-1897. <https://doi.org/10.1016/j.marpetgeo.2010.07.015>
- Fetter, M. R., De Ros, L. F., & Bruhn, C. H. L. (2009). Petrographic and seismic evidence for the depositional setting of giant turbidite reservoirs and the paleogeographic evolution of Campos Basin, offshore Brazil. *Marine and Petroleum Geology*, 26(6), 824-853. <https://doi.org/10.1016/j.marpetgeo.2008.07.008>
- Fossen, H., Schultz, R. A., Shipton, Z. K., & Mair, K. (2007). Deformation bands in sandstone: a review. *Journal of the Geological Society*, 164(4), 755-769. <https://doi.org/10.1144/0016-76492006-036>
- Galvão, M. S. (2018). *O papel da falhas e bandas de deformação sobre o fabric dos arenitos da Formação Resende (Eoceno, Rift Continental do Sudeste do Brasil) e seu impacto sobre o comportamento hidromecânico*. 184.
- Howell, J. A., Martinius, A. W., & Good, T. R. (2014). The application of outcrop analogues in geological modelling: a review, present status and future outlook. In A. W. Martinius, J. A. Howell, & T. R. Good (Eds.), *Sediment-Body Geometry and Heterogeneity: Analogue Studies for Modelling the Subsurface* (Vol. 387, n. 1, pp. 1-25). Geological Society. <https://doi.org/10.1144/SP387.12>
- Lima, L. F. A. (2017). *Confecção de uma ortofotoplanta planialtimétrica cadastral pelo método da aerofotogrametria digital utilizando imagens obtidas por VANT e comparação dos resultados com o método de topografia tradicional*. Estácio de Sá.
- Maciel, I. B., Mello, C. L., & Silva, A. T. (2017). Caracterização da deformação dútil em afloramento da Formação Resende, Bacia de Volta Redonda, Estado do Rio de Janeiro. *Geologia USP - Série Científica*, 17(3-4), 113-124. <https://doi.org/10.11606/issn.2316-9095v17-391>
- Mello, C. L., Barroso, E. V., Perosi, F. A., Ramos, R. R. C., Borges, A. F., & Polivanov, H. (2021). *Caracterização da deformação e de propriedades mecânicas e permoporosas de arenitos pouco consolidados*. Internal Report.
- Negrão, A. P., Mello, C. L., Ramos, R. R. C., Sanson, M. de S. R., Louro, V. H. A., & Bauli, P. G. (2020). Tectonosedimentary evolution of the Resende and Volta Redonda basins (Cenozoic, Central Segment of the Continental Rift of Southeastern Brazil). *Journal of South American Earth Sciences*, 104, 102789. <https://doi.org/10.1016/j.jsames.2020.102789>
- Negrão, A. P., Ramos, R. R. C., Mello, C. L., & Sanson, M. de S. R. (2015). Mapa geológico do cenozoico da região da bacia de Volta Redonda (RJ, segmento central do Rift Continental do Sudeste do Brasil): identificação de novos grabens e ocorrências descontínuas, e caracterização de estágios tectonosedimentares. *Brazilian Journal of Geology*, 45(2), 273-291. <https://doi.org/10.1590/23174889201500020007>
- Pei, Y., Paton, D. A., Knipe, R. J., & Wu, K. (2015). A review of fault sealing behaviour and its evaluation in siliciclastic rocks. *Earth-Science Reviews*, 150, 121-138. <https://doi.org/10.1016/j.earscirev.2015.07.011>
- Pontes, C. C. C., Nogueira, F. C. C., Bezerra, F. H. R., Balsamo, F., Miranda, T. S. de, Nicchio, M. A., Souza, J. A. B. de, & Carvalho, B. R. B. M. (2019). Petrophysical properties of deformation bands in high porous sandstones across fault zones in the Rio do Peixe Basin, Brazil. *International Journal of Rock Mechanics and Mining Sciences*, 114, 153-163. <https://doi.org/10.1016/j.ijrmms.2018.12.009>
- Riccomini, C. (1989). *O Rift continental do sudeste do Brasil*. Universidade de São Paulo.
- Riccomini, C., Sant'Anna, L. G., & Ferrari, A. L. (2004). Evolução geológica do rift continental do sudeste do Brasil. In F. F. M. Almeida (Ed.), *Geologia do Continente Sul-Americano: Evolução da Obra de Fernando Flávio Marques de Almeida* (p. 383-405).
- Rodrigues, R. de S., & Silva, F. C. A. (2018). Deformation bands and associated structures in the Tucano Basin, NE Brazil: A multiscale analysis. *Marine and Petroleum Geology*, 96, 202-213. <https://doi.org/10.1016/j.marpetgeo.2018.05.035>
- Rodrigues, Y. C. (2018). *Inunditos como análogos de reservatórios - Um exemplo nos depósitos gonduânicos triássicos do Gráben Arroio Moirão, RS*. Universidade do Rio Grande do Sul.
- Sanson, M. de S. R. (2006). *Sistemas deposicionais aluviais e tectônica rúptil na região de Volta Redonda (RJ) - Rift Continental do Sudeste do Brasil*. Universidade Federal do Rio de Janeiro.
- Sowek, G. A. (2013). *Caracterização de heterogeneidades em reservatórios fluviais a partir do estudo de análogo na formação Rio do Rasto, Bacia do Paraná*. Universidade Federal do Paraná.
- Stohler, R. de C. (2021). *Modelagem numérica 3D e simulação do impacto de bandas de deformação no escoamento em meio poroso*. Universidade Federal do Rio de Janeiro.
- Vogel, S. do N. (2018). *Caracterização macroscópica e microscópica de aspectos texturais e estruturais relacionados à deformação rúptil de arenitos pouco consolidados (Formação Resende, Bacia de Volta Redonda) e aspectos permoporosos associados*. Universidade Federal do Rio de Janeiro.
- Vogel, S. do N., Mello, C. L., & Silva, A. T. (2019). Aspectos Tomográficos e Microtomográficos de Feições de Deformação Rúptil em Arenitos Pouco Consolidados da Formação Resende (Bacia de Volta Redonda-RJ) Tomographic and Microtomographic Aspects of Brittle Deformation Features in the Poorly Lithified San. *Anuário do Instituto de Geociências*, 42(1), 759-768. https://doi.org/10.11137/2019_1_759_768